

Universal V-shaped temperature-pressure phase diagram in the iron-based superconductors KFe_2As_2 , RbFe_2As_2 , and CsFe_2As_2

F. F. Tafti,^{1,*} A. Ouellet,¹ A. Juneau-Fecteau,¹ S. Faucher,¹ M. Lapointe-Major,¹ N. Doiron-Leyraud,¹ A. F. Wang,² X.-G. Luo,² X. H. Chen,² and Louis Taillefer^{1,3,†}

¹Département de physique & RQMP, Université de Sherbrooke, Sherbrooke, Québec, Canada

²Hefei National Laboratory for Physical Sciences at Microscale and Department of Physics, University of Science and Technology of China, Hefei, China

³Canadian Institute for Advanced Research, Toronto, Ontario, Canada

(Received 18 December 2014; revised manuscript received 23 January 2015; published 17 February 2015)

We report a sudden reversal in the pressure dependence of T_c in the iron-based superconductor RbFe_2As_2 , at a critical pressure $P_c = 11$ kbar. Combined with our prior results on KFe_2As_2 and CsFe_2As_2 , we find a universal V-shaped phase diagram for T_c versus P in these fully hole-doped 122 materials, when measured relative to the critical point (P_c , T_c). From measurements of the upper critical field $H_{c2}(T)$ under pressure in KFe_2As_2 and RbFe_2As_2 , we observe the same twofold jump in $(1/T_c) (-\partial H_{c2}/\partial T)_{T_c}$ across P_c , compelling evidence for a sudden change in the structure of the superconducting gap. We argue that this change is due to a transition from one pairing state to another, with different symmetries on either side of P_c . We discuss a possible link between scattering and pairing, and a scenario where a d -wave state favored by high- Q scattering at low pressure changes to a state with s_{\pm} symmetry favored by low- Q scattering at high pressure.

DOI: 10.1103/PhysRevB.91.054511

PACS number(s): 74.70.Xa, 74.62.Fj, 61.50.Ks

I. INTRODUCTION

Pairing symmetry in the iron-based superconductors is controlled by the interband and the intraband interactions which are tunable by external parameters such as doping or pressure [1,2]. Recent theoretical works using a five-orbital tight-binding model show a near degeneracy between d and s_{\pm} pairing states in the 122 iron pnictides as a result of the multiorbital structure of the Cooper pairs and the near-nesting conditions [3,4]. Hydrostatic pressure is a clean tuning parameter that can modify the orbital overlap, the exchange interactions, and the band structure of metals. Given the near degeneracy between different pairing states, it is conceivable that the pairing symmetry of certain iron-based superconductors can be tuned by pressure. These ideas gained experimental relevance with our recent discovery of a V-shaped T - P phase diagram in KFe_2As_2 and CsFe_2As_2 , where T_c decreases initially as a function of pressure, then at a critical pressure P_c , it suddenly changes direction and increases [5,6]. Our results on KFe_2As_2 have been reproduced by other groups [7–9]. We interpreted the transition at P_c as a change of pairing state, possibly from d to s_{\pm} , where the decreasing T_c of the former meets the growing T_c of the latter at P_c , resulting in a V-shaped phase diagram.

In this paper, we present our discovery of a very similar V-shaped phase diagram in a third material: RbFe_2As_2 . We show that $\partial T_c/\partial P$ on both sides of P_c is the same in all three materials, which therefore share a universal V-shaped phase diagram. We show that the slope of $H_{c2}(T)$ jumps by a factor 2 across P_c , in a manner that also appears to be universal. This is compelling evidence for a sudden change in the gap structure [8], which we attribute to a change of pairing symmetry.

The Fermi surface of KFe_2As_2 is known in detail from quantum oscillations studies [10,11]. It consists of three quasi-

two-dimensional (quasi-2D) holelike cylinders centered on the Γ point, labeled α (small inner cylinder), ξ (middle cylinder), and β (large outer cylinder), as well as small cylindrical satellites at the corners of the Brillouin zone, labeled ε . There is also one small three-dimensional (3D) hole pocket at the Z point of the Brillouin zone [12]. The pairing symmetry of KFe_2As_2 at ambient pressure is the subject of ongoing debate. Laser ARPES experiments suggest a s_{\pm} state with eight line nodes on the ξ band and no nodes on the α and β bands [13,14]. By contrast, bulk measurements of thermal conductivity [15,16], heat capacity [17,18], and penetration depth [19,20] point to a d -wave state, with four line nodes on each of the Γ -centered Fermi pockets (α , ξ , and β).

II. METHODS

Single crystals of RbFe_2As_2 were grown using a self-flux method similar to KFe_2As_2 and CsFe_2As_2 [21,22]. Two samples of RbFe_2As_2 , labeled Samples A and B, were pressurized in a clamp cell and measured up to 22 kbar. The pressure was measured by monitoring the superconducting transition of a lead gauge placed beside the two samples in the clamp cell with a precision of ± 0.1 kbar. A 1/1 mixture of pentane and 3-methyl-1-butanol was used as the pressure medium. Measurements of resistivity and Hall effect were performed on both samples in an adiabatic demagnetization refrigerator using the standard six-contact configuration. Hall voltage was measured at plus and minus 10 T from $T = 20$ K to 1 K and antisymmetrized to calculate the Hall coefficient R_H . Excellent reproducibility was observed between the two samples. To avoid redundancy, we present the results from Sample A, unless otherwise mentioned.

III. RESULTS AND DISCUSSION

We have measured the pressure dependence of four quantities: the critical temperature T_c , the Hall coefficient R_H , the

*fazel.fallah.tafti@usherbrooke.ca
†louis.taillefer@usherbrooke.ca

upper critical field $H_{c2}(T)$, and the resistivity ρ . We present each measurement in turn, and discuss the implications.

A. Pressure dependence of T_c

Figure 1(a) shows our discovery of a sudden reversal in the pressure dependence of T_c in RbFe₂As₂ at a critical pressure $P_c = 11 \pm 1$ kbar. On the same figure, the green diamonds show T_c values reported previously for RbFe₂As₂ from ac susceptibility and μ SR measurements up to 10 kbar by Shermadini *et al.* [23]. These data are in excellent agreement with ours, but they stop at 10 kbar, just before P_c . By extrapolation, Shermadini *et al.* concluded that T_c would be fully suppressed at 19 kbar which is the natural expectation from a superconductor with one dominant pairing state.

We determined T_c from resistivity measurements using a $\rho = 0$ criterion. Figure 1(b) shows three representative resistivity curves at $P < P_c$, where T_c decreases by increasing pressure. Figure 1(c) shows three curves at $P > P_c$, where T_c reverses direction to increase by increasing pressure. T_c varies linearly near P_c from either side, resulting in a V-shaped phase diagram in RbFe₂As₂, similar to KFe₂As₂ and CsFe₂As₂ [5,6].

In Fig. 2, we compare the phase diagrams of KFe₂As₂, RbFe₂As₂, and CsFe₂As₂, with $P_c = 17.5$, 11, and 14 kbar,

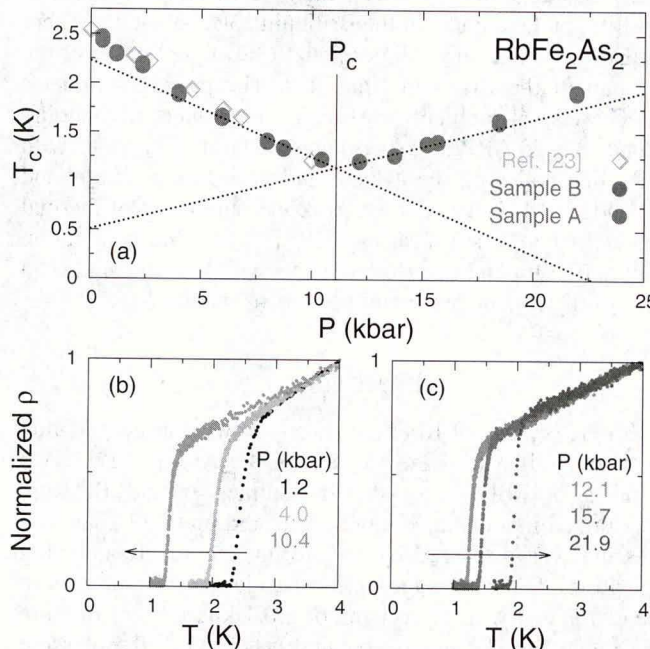


FIG. 1. (Color online) (a) Pressure dependence of T_c in RbFe₂As₂. The red and blue circles represent data from Samples A and B, respectively. T_c is defined as the temperature where $\rho = 0$. The critical pressure P_c marks the reversal in the T_c behavior from decreasing to increasing. Dotted lines are linear fits to the data in the range $P_c \pm 6$ kbar. The critical pressure $P_c = 11 \pm 1$ kbar is defined as the intersection of the two dotted lines. The green diamonds are data from Ref. [23], where T_c was measured by ac susceptibility and μ SR. (b) Three representative $\rho(T)$ curves in the low-pressure phase ($P < P_c$), from Sample A, normalized to unity at $T = 4$ K. The arrow shows that T_c decreases with increasing pressure. (c) Same as in (b) for the high-pressure phase ($P > P_c$). The arrow shows that T_c now increases with increasing pressure.

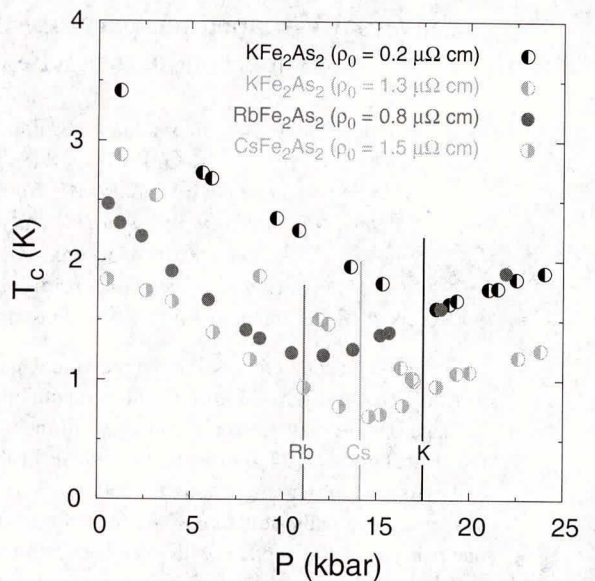


FIG. 2. (Color online) Temperature-pressure phase diagram of KFe₂As₂ (black and gray), RbFe₂As₂ (red), and CsFe₂As₂ (green). The residual resistivity ρ_0 of each sample is indicated. Comparing the black and gray points shows that P_c is unaffected by disorder. The three compounds show a T_c reversal at comparable critical pressures (color-coded vertical lines): $P_c = 17.5$, 11, and 14 kbar, in KFe₂As₂, RbFe₂As₂, and CsFe₂As₂, respectively. Data for KFe₂As₂ and CsFe₂As₂ are reproduced from Refs. [5,6], respectively. Error bars are no larger than the size of the points.

respectively. The black and gray symbols correspond to two samples of KFe₂As₂ with different disorder levels. Although the residual resistivity of the less pure sample ($\rho_0 = 1.3 \mu\Omega \text{ cm}$) is six times larger than that of the pure sample ($\rho_0 = 0.2 \mu\Omega \text{ cm}$), they have identical P_c . Hence, disorder does not affect the critical pressure.

Figure 2 also shows that the phase diagram of the less pure KFe₂As₂ sample (gray) is rigidly shifted down relative to the pure sample (black). Therefore, the low-pressure and the high-pressure superconducting phases have comparable (and large) sensitivity to disorder. The high sensitivity to disorder on both sides of P_c is incompatible with the standard s_{++} state, known to be resilient against disorder [27,28]. In KFe₂As₂ at ambient pressure, the steep drop of T_c as a function of controlled disorder was shown to be quantitatively consistent with the high sensitivity of a d -wave state to disorder [15,29,30]. Since the usual s_{\pm} state, with a sign change between pockets centered at different points in the Brillouin zone, is known to be much less sensitive to disorder than the d -wave state [30], it may be that the high-pressure phase is the s_{\pm}^h state proposed for KFe₂As₂ [31], where the gap changes sign between two of the Γ -centered pockets resulting in a higher sensitivity to disorder.

By measuring the lattice parameters of KFe₂As₂ under pressure, we showed in Ref. [6] that it takes about 30 kbar to tune the unit-cell volume and the As-Fe-As bond angle of CsFe₂As₂ to match those of KFe₂As₂. Therefore, if the structural parameters directly controlled P_c , one would expect the critical pressure of CsFe₂As₂ to be 30 kbar larger than that of KFe₂As₂. As shown in Fig. 2, the P_c of CsFe₂As₂ is in fact

TABLE I. Lattice parameters (a and c), unit-cell volume ($V = ca^2$), Sommerfeld coefficient in the specific heat (γ), critical temperature T_c at ambient pressure, T_c at P_c , and critical pressure P_c , for KFe_2As_2 , $RbFe_2As_2$, and $CsFe_2As_2$ [21,22,24–26]. As the atomic size of the alkali ion increases from K to Rb to Cs, lattice parameters, unit-cell volume, and the Sommerfeld coefficient systematically increase, while T_c systematically decreases. But, the critical pressure P_c does not follow these systematics: it decreases from K to Rb, then increases from Rb to Cs.

Material	a (Å)	c (Å)	V (Å 3)	γ (mJ/K 2 mol)	T_c ($P = 0$) (K)	T_c ($P = P_c$) (K)	P_c (kbar)
KFe_2As_2	3.84	13.84	204	99	3.6	1.6	17.5
$RbFe_2As_2$	3.86	14.45	215	128	2.5	1.2	11
$CsFe_2As_2$	3.89	15.07	228	184	1.8	0.7	14

less than the P_c of KFe_2As_2 . Table I lists the structural parameters of the three compounds at ambient pressure. Rb atoms are intermediate in size between K and Cs, hence, the lattice parameters of $RbFe_2As_2$ are in-between those of KFe_2As_2 and $CsFe_2As_2$. Figure 2 shows that the P_c of $RbFe_2As_2$ does not fall between those of the other two compounds. There is indeed no straightforward connection between lattice parameters, bond angles, or ionic sizes and the actual values of P_c in these three compounds. Interestingly, near optimal doping, in both 122 and 1111 families, there is indeed a straightforward connection between the structural parameters and T_c [32,33]. Near optimal doping, d wave is known to be a subdominant superconducting state while s wave is the dominant one [34]. The loss of this straightforward connection between superconductivity and structural parameters in the overdoped regime could result from a dominant d -wave state.

In Fig. 3, we make a direct comparison of the three V-shaped phase diagrams, by shifting each curve horizontally by P_c and vertically by T_c ($P = P_c$), so that the tip of the V coincides for

the three materials. Remarkably, we find the same, universal V-shaped phase diagram in the range $P_c \pm 10$ kbar. In other words, $(\partial T_c / \partial P)_{P < P_c}$ and $(\partial T_c / \partial P)_{P > P_c}$ are identical in the three materials. Such a universal phase diagram, independent of the alkali atom (A) in AFe_2As_2 and of the different structural parameters, poses a clear challenge to our understanding of multiband superconductivity.

B. Pressure dependence of R_H

In our previous work on KFe_2As_2 and $CsFe_2As_2$, we showed that the V-shaped pressure dependence of T_c is not accompanied by any abrupt changes in the normal-state properties. In particular, the zero-temperature limit of the Hall coefficient $R_H(0)$ was found constant in both materials as a function of pressure across P_c , ruling out a sudden change in the Fermi surface, i.e., a Lifshitz transition [5,6]. We concluded that the phase transition at P_c is not triggered by some change in the Fermi surface, and is instead associated with a change in the superconducting state itself. This was confirmed by quantum oscillation measurements on KFe_2As_2 under pressure, which found a smooth evolution of the oscillation frequencies and cyclotron masses across P_c [7].

Figure 4(a) shows the temperature dependence of R_H in $RbFe_2As_2$, at various pressures. The low-temperature data go as T^2 , allowing us to extract $R_H(0)$ from a linear fit of $R_H(T)$ versus T^2 , as shown in Fig. 4(b). The $R_H(0)$ values are plotted as a function of pressure in Fig. 4(c). We find a small but smooth variation in $R_H(0)$, with no anomaly at $P_c = 11$ kbar, very different from the steplike structure expected of a typical Lifshitz transition [35].

In Fig. 5, we summarize the results of our Hall measurements in the three materials. In KFe_2As_2 and $CsFe_2As_2$, $R_H(0)$ is completely flat with pressure. In $RbFe_2As_2$, there is a broad structure in $R_H(0)$ and a straight line does not go through all data points. We attribute this broad feature to a smooth evolution of the Fermi surface parameters under pressure. Taken together, these Hall data make a compelling case that the universal V-shaped T_c versus P curve of Fig. 3 is not shaped by a sudden change in the Fermi surface at P_c .

C. Pressure dependence of H_{c2}

Measurements of the upper critical field H_{c2} in KFe_2As_2 under pressure can be used to provide evidence for a change of gap structure across P_c . Recently, Taufour *et al.* found a change of regime in the dependence of the quantity $(1/T_c) (-\partial H_{c2}/\partial T)_{T_c}$ as a function of the A coefficient

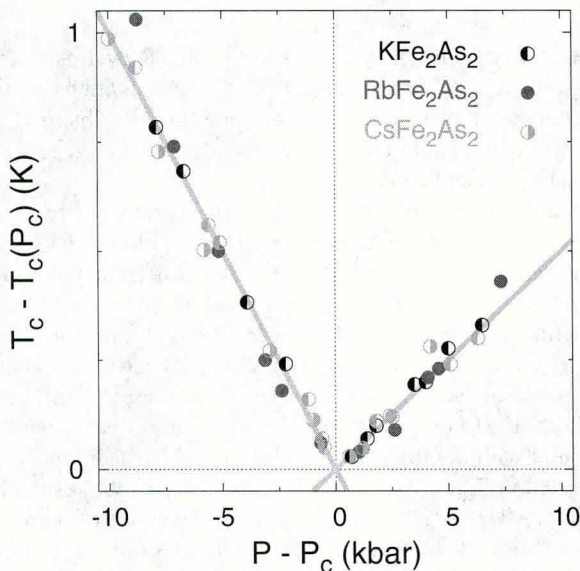


FIG. 3. (Color online) Universal V-shaped phase diagram of AFe_2As_2 , where $A = K$ (black and gray), Rb (red), and Cs (green). Data points from Fig. 2 are replotted with pressure values shifted by the respective critical pressures ($P_c = 17.5, 11$, and 14 kbar, for $A = K, Rb$, and Cs) and T_c values shifted by the respective values of T_c at P_c (1.6, 1.2, and 0.7 K, for $A = K, Rb$, and Cs). Error bars are no larger than the size of the points. The yellow lines are linear fits on either side of P_c .

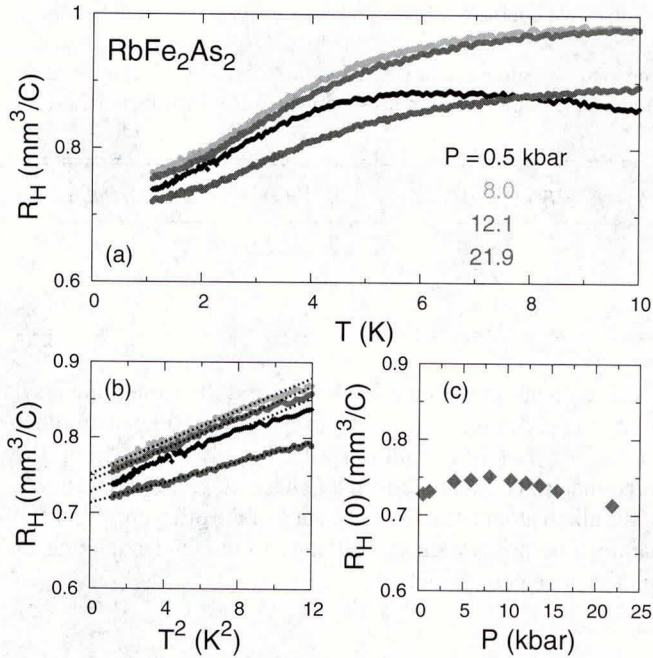


FIG. 4. (Color online) (a) Temperature dependence of the Hall coefficient $R_H(T)$ in RbFe_2As_2 at four pressures as indicated. (b) $R_H(T)$ plotted versus T^2 for the same pressures as in (a), at low temperature. The dotted lines are linear fits from which the zero-temperature limit of the Hall coefficient $R_H(0)$ is obtained at each pressure. (c) $R_H(0)$ plotted as a function of pressure, showing a small but smooth variation. Vertical and horizontal error bars are no larger than the size of the points. Vertical error bars come from the uncertainty in the T^2 fits in (b), associated with changing the fitting interval.

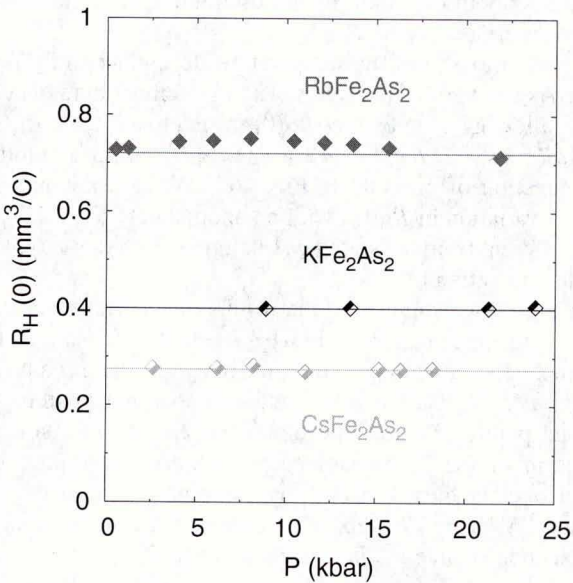


FIG. 5. (Color online) The zero-temperature limit of the Hall coefficient $R_H(0)$, plotted for the three materials $A\text{Fe}_2\text{As}_2$, where $A = \text{K}$ (black), Rb (red), and Cs (green). Vertical and horizontal error bars are no larger than the size of the points. Within error bars, $R_H(0)$ is constant for KFe_2As_2 and CsFe_2As_2 and nearly so for RbFe_2As_2 . Horizontal lines are a guide to the eye. Data for KFe_2As_2 and CsFe_2As_2 are reproduced from Refs. [5,6], respectively.

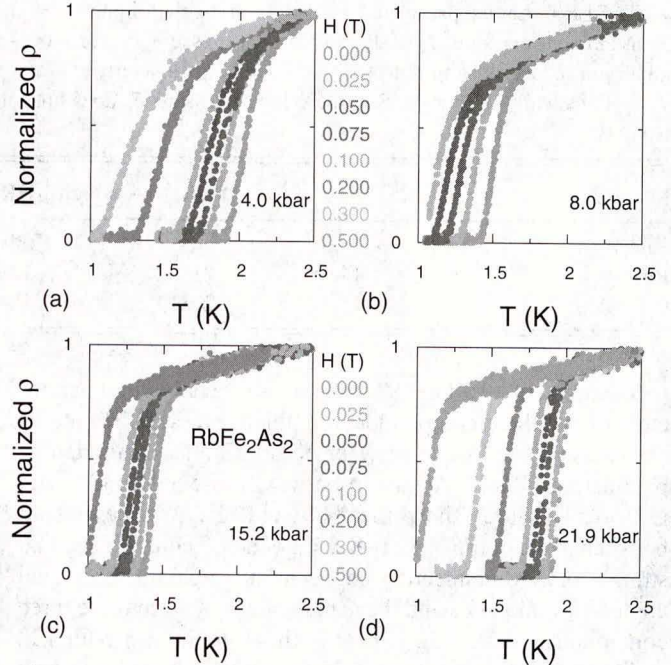


FIG. 6. (Color online) Resistivity $\rho(T)$ of RbFe_2As_2 normalized to unity at $T = 2.5$ K, at $P = 4.0, 8.0, 15.2$, and 21.9 kbar. The color of each curve corresponds to a field H as indicated. At each field, T_c is defined from the resistive transition using the criterion $\rho = 0$. This yields the curves of H_{c2} vs T in Fig. 7(a). Note that the width of the transition is larger in the low-pressure phase [e.g., in (a)] compared to the high-pressure phase [e.g., in (d)] because $\partial T_c/\partial P$ is almost two times higher in the low-pressure phase (Fig. 3). Therefore, a small pressure gradient across the sample in the pressure cell generates wider transition in the low-pressure phase.

of resistivity from $\rho(T) = \rho_0 + AT^2$ [8]. They linked this change of regime to a change in the k_z corrugations of the superconducting gap at the critical pressure P_c . Inspired by their work, we explored the pressure dependence of H_{c2} in both KFe_2As_2 and RbFe_2As_2 .

At any given pressure, we used measurements of $\rho(T)$ at different fields to determine $H_{c2}(T)$. Figure 6 shows normalized $\rho(T)$ curves in RbFe_2As_2 at different fields, for four representative pressures, below and above $P_c = 11$ kbar. We define T_c at each field from the resistive transition using the $\rho = 0$ criterion, then plot those T_c values versus H at each pressure, to arrive at the H - T curves shown in Fig. 7(a).

The four $H_{c2}(T)$ curves in Fig. 7(a) should be viewed in two pairs with comparable T_c values on either side of P_c , as illustrated in Fig. 7(b). Figure 7(c) summarizes the results by plotting $(-\partial H_{c2}/\partial T)_{T_c}$ versus T_c for the two pairs of points at $T_c \simeq 1.4$ and 1.9 K. At each value of T_c , the full symbol lies above the empty one, showing that the high-pressure phase is more robust against the magnetic field than the low-pressure phase. To obtain $(-\partial H_{c2}/\partial T)_{T_c}$ in RbFe_2As_2 , we made linear fits to the H - T curves in Fig. 7(a) near T_c .

Figure 8 shows $(1/T_c)(-\partial H_{c2}/\partial T)_{T_c}$ versus $(P - P_c)$ for both RbFe_2As_2 and KFe_2As_2 . In total, we measured $H_{c2}(T)$ at six different pressures, corresponding to the six red squares in Fig. 8. The four black data points in Fig. 8 come from similar measurements on KFe_2As_2 , from the $H_{c2}(T)$ curves

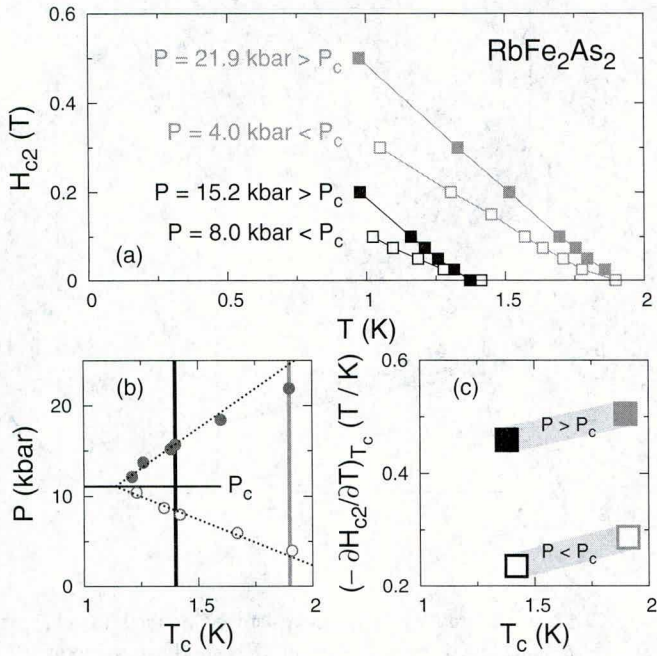


FIG. 7. (Color online) The full symbols in this figure represent the high-pressure phase ($P > P_c$) and the empty symbols represent the low-pressure phase ($P < P_c$). (a) $H_{c2}(T)$ in RbFe_2As_2 at four pressures. The light blue pair of curves starts from $T_c \simeq 1.9 \text{ K}$ and the dark blue pair starts from $T_c \simeq 1.4 \text{ K}$, at $H = 0$. At a given T_c , the low-pressure curve has a lower slope compared to the high-pressure one. (b) The V-shaped phase diagram of RbFe_2As_2 , rotated by 90° , with lines that cut through the “V” at pairs of pressures corresponding to the light blue and the dark blue curves in panel (a). (c) $(-\partial H_{c2}/\partial T)|_{T_c}$ is extracted from linear fits to the curves in panel (a) near T_c and plotted against T_c . The light blue pair of points is vertically aligned at $T_c \simeq 1.9 \text{ K}$ and the dark blue pair at $T_c \simeq 1.4 \text{ K}$ corresponding to the vertical lines in panel (b). Error bars are no larger than the size of the points. We observe that consistently $(-\partial H_{c2}/\partial T)|_{T_c}$ is larger in the high-pressure phase.

shown in Fig. 9. The magnitude of $(1/T_c)(-\partial H_{c2}/\partial T)|_{T_c}$ is the same in the two materials, on both sides of P_c , revealing a second universal property of the pressure-induced transition: a twofold jump in $(1/T_c)(-\partial H_{c2}/\partial T)|_{T_c}$ at $P = P_c$ (Fig. 8).

The Helfand-Werthamer theory, modified for superconductors with anisotropic gap structures [36], relates the quantity $(1/T_c)(-\partial H_{c2}/\partial T)|_{T_c}$ to the gap dispersion Ω and the anisotropic Fermi velocity v_0 through the relation

$$\frac{1}{T_c} \left(\frac{-\partial H_{c2}}{\partial T} \right)_{T_c} = \frac{16\pi\phi_0 k_B^2}{7\zeta(3)\hbar^2} \frac{1}{\langle \Omega^2 \mu_c \rangle} \frac{1}{v_0^2}, \quad (1)$$

where ϕ_0 , \hbar , and k_B are the magnetic flux quantum, the Planck constant, and the Boltzmann constant. μ_c and v_0 relate to the Fermi surface parameters according to

$$\mu_c = \frac{v_x^2 + v_y^2}{v_0^2} \quad \text{and} \quad v_0^3 = \frac{2E_F^2}{\pi^2\hbar^3 N(0)}, \quad (2)$$

where E_F and $N(0)$ are the Fermi energy and the density of states at the Fermi level. Fermi velocity is not a constant at anisotropic Fermi surfaces, hence, a characteristic constant velocity v_0 is defined in Eq. (2) applicable to anisotropic Fermi

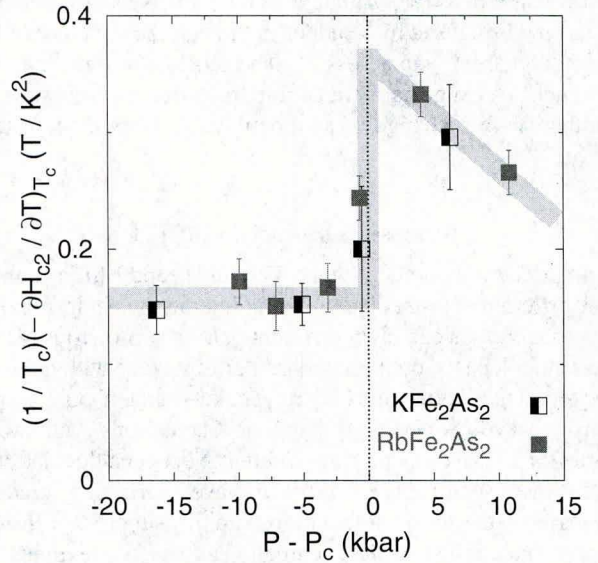


FIG. 8. (Color online) $(1/T_c)(-\partial H_{c2}/\partial T)|_{T_c}$ as a function of $P - P_c$ in RbFe_2As_2 (red squares) and KFe_2As_2 (black squares). The two materials are seen to display the same behavior, with the same magnitude on both sides of P_c . The thick gray line is a guide to the eye. A twofold jump is observed at $P = P_c$, revealing a clear difference between the low-pressure phase ($P - P_c < 0$) and the high-pressure phase ($P - P_c > 0$).

surfaces [36]. For the isotropic case, one recovers $v_0 = v_F$. The function Ω describes the momentum dependence of the superconducting gap: $\Delta = \Psi(\mathbf{r}, \mathbf{T})\Omega(\mathbf{k}_F)$. The averages $\langle \dots \rangle$ are taken over the Fermi surface.

Given that quantum oscillation measurements in KFe_2As_2 under pressure show a smooth evolution of v_F across P_c [7], the twofold jump in $(1/T_c)(-\partial H_{c2}/\partial T)|_{T_c}$ observed at P_c can only

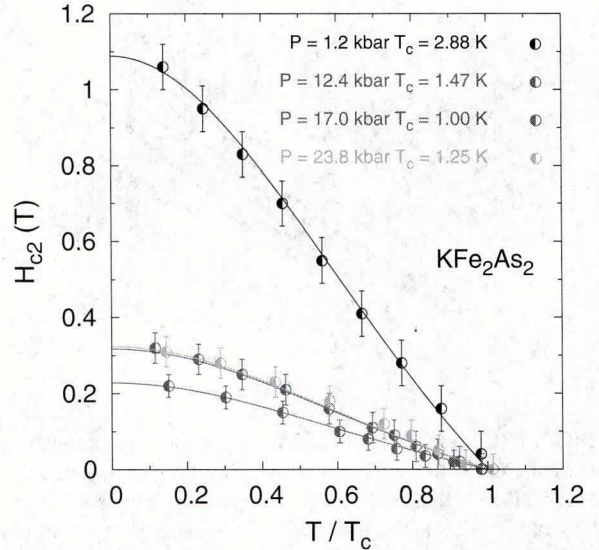


FIG. 9. (Color online) $H_{c2}(T)$ in KFe_2As_2 plotted as a function of T/T_c . At each pressure, $(-\partial H_{c2}/\partial T)|_{T_c}$ is obtained by fitting a line to the $H_{c2}(T)$ curve near T_c . The resulting $(1/T_c)(-\partial H_{c2}/\partial T)|_{T_c}$ values are the black data points in Fig. 8. Solid lines are a guide to the eye.

be the result of a sudden change in the gap dispersion function Ω in Eq. (1), caused by a sudden change in the structure of the superconducting gap across P_c . The most natural mechanism for such a change is a transition from one pairing state to another, with a change of symmetry, e.g., from d wave to s wave.

D. Pressure dependence of $\rho(T)$

In a recent theoretical work, Fernandes and Millis showed how different spin-mediated pairing interactions in iron-based superconductors can favor different pairing symmetries [4]. In their model, based on the standard Fermi surface with holelike pockets at the Γ point and electron pockets at the X points, spin density wave (SDW) type magnetic fluctuations, with wave vector $(\pi, 0)$, favor s_{\pm} pairing, whereas Néel-type fluctuations, with wave vector (π, π) , favor d -wave pairing. A gradual increase in the (π, π) fluctuations rapidly suppresses the s_{\pm} superconducting state and eventually causes a phase transition from the s_{\pm} state to a d -wave state, producing a V-shaped phase diagram of T_c versus tuning parameter [strength of (π, π) correlations] [4].

It is conceivable that two such competing interactions are at play in AFe_2As_2 , with pressure tilting the balance in favor of one versus the other. We explore such a scenario by looking at how the inelastic scattering evolves with pressure, measured via the inelastic resistivity, defined as $\rho(T = 20 K) - \rho_0$. Figure 10 shows the temperature dependence of resistivity, at six representative pressures, in $RbFe_2As_2$. The residual resistivity ρ_0 comes from a power-law fit to the resistivity

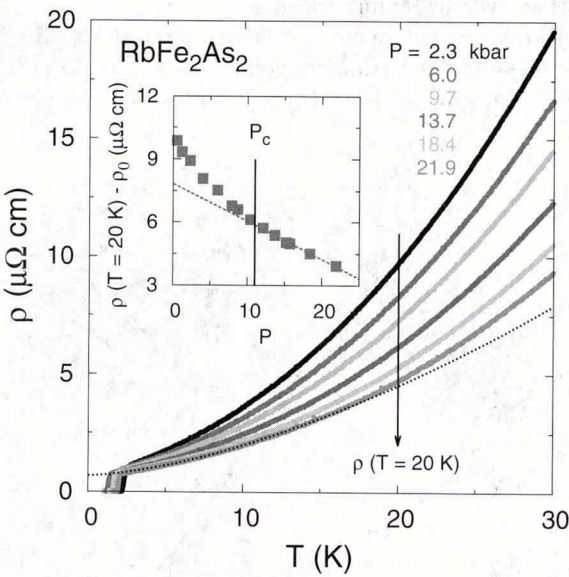


FIG. 10. (Color online) Resistivity of sample A as a function of temperature up to 30 K, at six representative pressures, as indicated. The vertical arrow that cuts through the resistivity curves at $T = 20$ K defines $\rho(T = 20$ K). The black dotted line is a power-law fit to the resistivity curve at $P = 21.9$ kbar, in the interval from $T = 3$ K to 15 K. We define the residual resistivity ρ_0 as the zero-temperature limiting value of this fit. The inset shows the pressure dependence of the inelastic resistivity $\rho(T = 20$ K) $- \rho_0$. The vertical arrow in the inset shows $P_c = 11$ kbar. The red dashed line is a linear fit to the inelastic resistivity as a function of pressure at $P > P_c$.

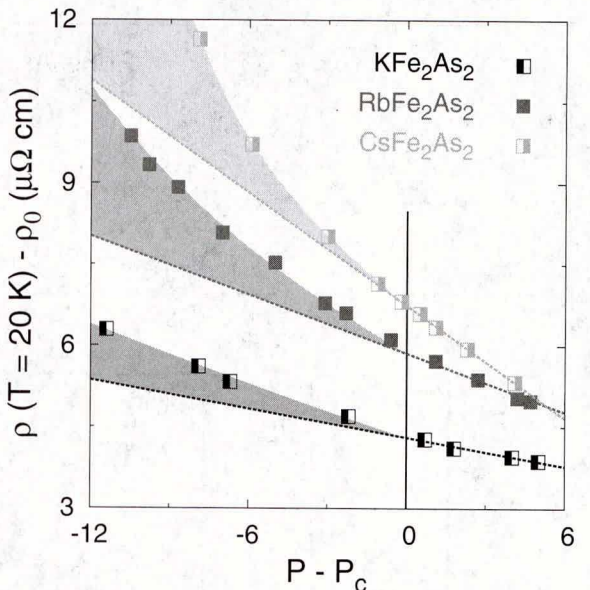


FIG. 11. (Color online) Inelastic resistivity defined as $\rho(T = 20$ K) $- \rho_0$ and plotted versus $P - P_c$ in KFe_2As_2 (black symbols, $P_c = 17.5$ kbar), $RbFe_2As_2$ (red symbols, $P_c = 11$ kbar), and $CsFe_2As_2$ (green symbols, $P_c = 14$ kbar). Dashed lines are linear fits to the data at $P - P_c > 0$ showing that the inelastic resistivity scales linearly with pressure in the high-pressure phase above P_c . As the pressure is lowered below P_c , a new channel contributes to the inelastic resistivity of AFe_2As_2 shown as shaded areas in gray, red, and green for $A = K$, Rb , and Cs . The vertical black line marks $P = P_c$.

at any pressure, of the form $\rho = \rho_0 + AT^n$. The resulting ρ_0 does not change with pressure. $\rho(T = 20$ K) is the value of the resistivity at $T = 20$ K, at any given pressure. Through the same procedure, we extracted ρ_0 and $\rho(T = 20$ K) as a function of pressure in KFe_2As_2 and $CsFe_2As_2$, from published data [5,6]. In Fig. 11, the inelastic resistivity $\rho(T = 20$ K) $- \rho_0$ is plotted as a function of $P - P_c$. In all three materials, at $P - P_c > 0$, the inelastic resistivity varies linearly with pressure. As P drops below P_c in the low-pressure phase ($P - P_c < 0$), the inelastic resistivity shows a clear rise over and above the linear regime. Figure 11 therefore suggests a connection between the transition in the pressure dependence of T_c and the appearance of an additional inelastic scattering channel. Note that our choice of $T = 20$ K to define the inelastic resistivity is arbitrary; resistivity cuts at any other temperature above T_c give qualitatively similar results.

Now, the intraband inelastic scattering wave vectors that favor d -wave pairing in KFe_2As_2 are large- Q processes where Q is the momentum transfer [37]. By contrast, theoretical calculations show that the s_{\pm}^h pairing state, which changes sign between the α and the ξ hole pockets, is favored by small- Q interband interactions [31]. Therefore, one scenario in which to understand the evolution in the inelastic resistivity with pressure (Fig. 11), and its link to the T_c reversal, is the following. At low pressure, the large- Q scattering processes that favor d -wave pairing make a substantial contribution to the resistivity, as they produce a large change in momentum. These weaken with pressure, causing a decrease in both T_c and the resistivity. This decrease persists until the low- Q processes

that favor s_{\pm}^h pairing, less visible in the resistivity, come to dominate, above P_c .

IV. SUMMARY

In summary, we report a universal V-shaped pressure dependence of T_c in AFe_2As_2 with $A = K$, Rb , and Cs . Remarkably, the temperature-pressure superconducting phase diagram of these fully hole-doped iron arsenides is universal, unaffected by a change in the alkali atom A , with its concomitant changes in structural parameters. In the absence of any sudden change in the Fermi surface across the critical pressure P_c , we interpret the T_c reversal at P_c as a transition from one pairing state to another. The observation of a sudden change in the upper critical field $H_{c2}(T)$, which also appears to be universal in that it is identical in $RbFe_2As_2$ and KFe_2As_2 , is compelling evidence of a sudden change in the structure of the superconducting gap across P_c . Our proposal is a d -wave state below P_c and a so-called s_{\pm}^h state, where the gap changes sign between Γ -centered hole pockets, above P_c . Our study of the pressure dependence of resistivity in KFe_2As_2 , $CsFe_2As_2$, and $RbFe_2As_2$ reveals a possible link between T_c and inelastic

scattering. As the pressure is lowered, the large- Q inelastic scattering processes that favor d -wave pairing grow until at a critical pressure P_c they cause a change of pairing symmetry from s wave to d wave.

ACKNOWLEDGMENTS

We thank J. Carbotte, A. V. Chubukov, J. P. Clancy, R. M. Fernandes, M. Franz, Y.-J. Kim, C. Meingast, A. J. Millis, R. Prozorov, P. Richard, M. A. Tanatar, V. Taufour, I. Vekhter, and H. von Löhneysen for helpful discussions, as well as B. Vincent and S. Fortier for assistance with the experiments. The work at Sherbrooke was supported by the Canadian Institute for Advanced Research and a Canada Research Chair and it was funded by National Science and Engineering Research Council of Canada, Fonds de Recherche du Québec Nature et Technologies, and Canada Foundation for Innovation. Work done in China was supported by the National Natural Science Foundation of China (Grant No. 11190021), the Strategic Priority Research Program (B) of the Chinese Academy of Sciences, and the National Basic Research Program of China.

-
- [1] A. Chubukov, Pairing mechanism in Fe-based superconductors, *Annu. Rev. Condens. Matter Phys.* **3**, 57 (2012).
 - [2] P. J. Hirschfeld, M. M. Korshunov, and I. I. Mazin, Gap symmetry and structure of Fe-based superconductors, *Rep. Prog. Phys.* **74**, 124508 (2011).
 - [3] S. Graser, T. A. Maier, P. J. Hirschfeld, and D. J. Scalapino, Near-degeneracy of several pairing channels in multiorbital models for the Fe pnictides, *New J. Phys.* **11**, 025016 (2009).
 - [4] R. M. Fernandes and A. J. Millis, Suppression of superconductivity by Néel-type magnetic fluctuations in the iron pnictides, *Phys. Rev. Lett.* **110**, 117004 (2013).
 - [5] F. F. Tafti, A. Juneau-Fecteau, M.-E. Delage, S. René de Cotret, J.-P. Reid, A. F. Wang, X.-G. Luo, X. H. Chen, N. Doiron-Leyraud, and L. Taillefer, Sudden reversal in the pressure dependence of T_c in the iron-based superconductor KFe_2As_2 , *Nat. Phys.* **9**, 349 (2013).
 - [6] F. F. Tafti, J. P. Clancy, M. Lapointe-Major, C. Collignon, S. Faucher, J. A. Sears, A. Juneau-Fecteau, N. Doiron-Leyraud, A. F. Wang, X.-G. Luo, X. H. Chen, S. Desgreniers, Y.-J. Kim, and L. Taillefer, Sudden reversal in the pressure dependence of T_c in the iron-based superconductor $CsFe_2As_2$: A possible link between inelastic scattering and pairing symmetry, *Phys. Rev. B* **89**, 134502 (2014).
 - [7] T. Terashima, K. Kihou, K. Sugii, N. Kikugawa, T. Matsumoto, S. Ishida, C.-H. Lee, A. Iyo, H. Eisaki, and S. Uji, Two distinct superconducting states in KFe_2As_2 under high pressure, *Phys. Rev. B* **89**, 134520 (2014).
 - [8] V. Taufour, N. Foroozani, M. A. Tanatar, J. Lim, U. Kaluarachchi, S. K. Kim, Y. Liu, T. A. Lograsso, V. G. Kogan, R. Prozorov, S. L. Bud'ko, J. S. Schilling, and P. C. Canfield, Upper critical field of KFe_2As_2 under pressure: A test for the change in the superconducting gap structure, *Phys. Rev. B* **89**, 220509 (2014).
 - [9] V. Grinenko, W. Schottenhamel, A. U. B. Wolter, D. V. Efremov, S.-L. Drechsler, S. Aswartham, M. Kumar, S. Wurmehl, M. Roslova, I. V. Morozov, B. Holzapfel, B. Büchner, E. Ahrens, S. I. Troyanov, S. Köhler, E. Gati, S. Knöner, N. H. Hoang, M. Lang, F. Ricci, and G. Profeta, Superconducting properties of $K_{1-x}Na_xFe_2As_2$ under pressure, *Phys. Rev. B* **90**, 094511 (2014).
 - [10] T. Terashima, M. Kimata, N. Kurita, H. Satsukawa, A. Harada, K. Hazama, M. Imai, A. Sato, K. Kihou, C.-H. Lee, H. Kito, H. Eisaki, A. Iyo, T. Saito, H. Fukazawa, Y. Kohori, H. Harima, and S. Uji, Fermi surface and mass enhancement in KFe_2As_2 from de Haas-van Alphen effect measurements, *J. Phys. Soc. Jpn.* **79**, 053702 (2010).
 - [11] T. Terashima, N. Kurita, M. Kimata, M. Tomita, S. Tsuchiya, M. Imai, A. Sato, K. Kihou, C.-H. Lee, H. Kito, H. Eisaki, A. Iyo, T. Saito, H. Fukazawa, Y. Kohori, H. Harima, and S. Uji, Fermi surface in KFe_2As_2 determined via de Haas-van Alphen oscillation measurements, *Phys. Rev. B* **87**, 224512 (2013).
 - [12] Diego A. Zocco, Kai Grube, Felix Eilers, Thomas Wolf, and Hilbert v. Löhneysen, Fermi surface of KFe_2As_2 from quantum oscillations in magnetostriction, *J. Phys. Soc. Jpn.* **3**, 015007 (2014).
 - [13] K. Okazaki, Y. Ota, Y. Kotani, W. Malaeb, Y. Ishida, T. Shimojima, T. Kiss, S. Watanabe, C.-T. Chen, K. Kihou, C. H. Lee, A. Iyo, H. Eisaki, T. Saito, H. Fukazawa, Y. Kohori, K. Hashimoto, T. Shibauchi, Y. Matsuda, H. Ikeda, H. Miyahara, R. Arita, A. Chainani, and S. Shin, Octet-line node structure of superconducting order parameter in KFe_2As_2 , *Science* **337**, 1314 (2012).
 - [14] D. Watanabe, T. Yamashita, Y. Kawamoto, S. Kurata, Y. Mizukami, T. Ohta, S. Kasahara, M. Yamashita, T. Saito, H. Fukazawa, Y. Kohori, S. Ishida, K. Kihou, C. H. Lee, A. Iyo, H. Eisaki, A. B. Vorontsov, T. Shibauchi, and Y. Matsuda, Doping evolution of the quasiparticle excitations in heavily hole-doped $Ba_{1-x}K_xFe_2As_2$: A possible superconducting gap with signreversal between hole pockets, *Phys. Rev. B* **89**, 115112 (2014).

- [15] J.-P. Reid, M. A. Tanatar, A. Juneau-Fecteau, R. T. Gordon, S. R. de Cotret, N. Doiron-Leyraud, T. Saito, H. Fukazawa, Y. Kohori, K. Kihou, C. H. Lee, A. Iyo, H. Eisaki, R. Prozorov, and L. Taillefer, Universal heat conduction in the iron arsenide superconductor KFe_2As_2 : Evidence of a d -wave state, *Phys. Rev. Lett.* **109**, 087001 (2012).
- [16] J.-P. Reid, A. Juneau-Fecteau, R. T. Gordon, S. René de Cotret, N. Doiron-Leyraud, X.-G. Luo, H. Shakeripour, J. Chang, M. A. Tanatar, H. Kim, R. Prozorov, T. Saito, H. Fukazawa, Y. Kohori, K. Kihou, C. H. Lee, A. Iyo, H. Eisaki, B. Shen, H.-H. Wen, and L. Taillefer, From d -wave to s -wave pairing in the iron-pnictide superconductor $(Ba,K)Fe_2As_2$, *Supercond. Sci. Technol.* **25**, 084013 (2012).
- [17] M. Abdel-Hafiez, V. Grinenko, S. Aswartham, I. Morozov, M. Roslova, O. Vakaliuk, S. Johnston, D. V. Efremov, J. van den Brink, H. Rosner, M. Kumar, C. Hess, S. Wurmehl, A. U. B. Wolter, B. Büchner, E. L. Green, J. Wosnitza, P. Vogt, A. Reifenberger, C. Enss, M. Hempel, R. Klingeler, and S.-L. Drechsler, Evidence of d -wave superconductivity in $K_{1-x}Na_xFe_2As_2$ ($x = 0, 0.1$) single crystals from low-temperature specific-heat measurements, *Phys. Rev. B* **87**, 180507(R) (2013).
- [18] V. Grinenko, D. V. Efremov, S.-L. Drechsler, S. Aswartham, D. Gruner, M. Roslova, I. Morozov, K. Nenkov, S. Wurmehl, A. U. B. Wolter, B. Holzapfel, and B. Büchner, Superconducting specific-heat jump $\Delta C_{el} \propto T_c^\beta$ ($\beta \approx 2$) for $K_{1-x}Na_xFe_2As_2$, *Phys. Rev. B* **89**, 060504(R) (2014).
- [19] K. Hashimoto, A. Serafin, S. Tonegawa, R. Katsumata, R. Okazaki, T. Saito, H. Fukazawa, Y. Kohori, K. Kihou, C. H. Lee, A. Iyo, H. Eisaki, H. Ikeda, Y. Matsuda, A. Carrington, and T. Shibauchi, Evidence for superconducting gap nodes in the zone-centered hole bands of KFe_2As_2 from magnetic penetration-depth measurements, *Phys. Rev. B* **82**, 014526 (2010).
- [20] H. Kim, M. A. Tanatar, Y. Liu, Z. C. Sims, C. Zhang, P. Dai, T. A. Lograsso, and R. Prozorov, Evolution of london penetration depth with scattering in single crystals of $K_{1-x}Na_xFe_2As_2$, *Phys. Rev. B* **89**, 174519 (2014).
- [21] A. F. Wang, B. Y. Pan, X. G. Luo, F. Chen, Y. J. Yan, J. J. Ying, G. J. Ye, P. Cheng, X. C. Hong, S. Y. Li, and X. H. Chen, Calorimetric study of single-crystal $CsFe_2As_2$, *Phys. Rev. B* **87**, 214509 (2013).
- [22] Z. Zhang, A. F. Wang, X. C. Hong, J. Zhang, B. Y. Pan, J. Pan, Y. Xu, X. G. Luo, X. H. Chen, and S. Y. Li, Heat transport in $RbFe_2As_2$ single crystal: Evidence for nodal superconducting gap, *Phys. Rev. B* **91**, 024502 (2015).
- [23] Z. Shermadini, H. Luetkens, A. Maisuradze, R. Khasanov, Z. Bukowski, H.-H. Klauss, and A. Amato, Superfluid density and superconducting gaps of $RbFe_2As_2$ as a function of hydrostatic pressure, *Phys. Rev. B* **86**, 174516 (2012).
- [24] K. Sasimal, B. Lv, B. Lorenz, A. M. Guloy, F. Chen, Y.-Y. Xue, and C.-W. Chu, Superconducting Fe-based compounds ($A_{1-x}Sr_x$) Fe_2As_2 with $A=K$ and Cs with transition temperatures up to 37 K, *Phys. Rev. Lett.* **101**, 107007 (2008).
- [25] M. Aftabuzzaman and A. K. M. A. Islam, New superconducting $RbFe_2As_2$: A first-principles investigation, *Phys. C (Amsterdam)* **470**, 202 (2010).
- [26] F. Hardy, A. E. Böhmer, D. Aoki, P. Burger, T. Wolf, P. Schweiss, R. Heid, P. Adelmann, Y. X. Yao, G. Kotliar, J. Schmalian, and C. Meingast, Evidence of strong correlations and coherence-incoherence crossover in the iron pnictide superconductor KFe_2As_2 , *Phys. Rev. Lett.* **111**, 027002 (2013).
- [27] P. W. Anderson, Theory of dirty superconductors, *J. Phys. Chem. Solids* **11**, 26 (1959).
- [28] R. Prozorov, M. Konczykowski, M. A. Tanatar, A. Thaler, S. L. Bud'ko, P. C. Canfield, V. Mishra, and P. J. Hirschfeld, Effect of electron irradiation on superconductivity in single crystals of $Ba(Fe_{1-x}Ru_x)_2As_2$ ($x = 0.24$), *Phys. Rev. X* **4**, 041032 (2014).
- [29] A. F. Wang, S. Y. Zhou, X. G. Luo, X. C. Hong, Y. J. Yan, J. J. Ying, P. Cheng, G. J. Ye, Z. J. Xiang, S. Y. Li, and X. H. Chen, Anomalous impurity effects in the iron-based superconductor KFe_2As_2 , *Phys. Rev. B* **89**, 064510 (2014).
- [30] K. Kirshenbaum, S. R. Saha, S. Zieman, T. Drye, and J. Paglione, Universal pair-breaking in transition-metalsubstituted iron-pnictide superconductors, *Phys. Rev. B* **86**, 140505 (2012).
- [31] S. Maiti, M. M. Korshunov, and A. V. Chubukov, Gap symmetry in KFe_2As_2 and the $\cos 4\theta$ gap component in $LiFeAs$, *Phys. Rev. B* **85**, 014511 (2012).
- [32] M. Rotter, M. Pangerl, M. Tegel, and D. Johrendt, Superconductivity and crystal structures of $(Ba_{1-x}K_x)Fe_2As_2$ ($x = 0.1$), *Angew. Chem., Int. Ed.* **47**, 7949 (2008).
- [33] K. Miyoshi, E. Kojima, S. Ogawa, Y. Shimojo, and J. Takeuchi, Superconductivity under pressure in $RFeAsO_{1-x}F_x$ ($R = La$, Ce-Sm) by dc magnetization measurements, *Phys. Rev. B* **87**, 235111 (2013).
- [34] F. Kretzschmar, B. Muschler, T. Böhm, A. Baum, R. Hackl, H.-H. Wen, V. Tsurkan, J. Deisenhofer, and A. Loidl, Raman-scattering detection of nearly degenerate s -wave and d -wave pairing channels in iron-based $Ba_{0.6}K_{0.4}Fe_2As_2$ and $Rb_{0.8}Fe_{1.6}Se_2$ superconductors, *Phys. Rev. Lett.* **110**, 187002 (2013).
- [35] C. Liu, T. Kondo, R. M. Fernandes, A. D. Palczewski, E. D. Mun, N. Ni, A. N. Thaler, A. Bostwick, E. Rotenberg, J. Schmalian, S. L. Bud'ko, P. C. Canfield, and A. Kaminski, Evidence for a Lifshitz transition in electron-doped iron arsenic superconductors at the onset of superconductivity, *Nat. Phys.* **6**, 419 (2010).
- [36] V. G. Kogan and R. Prozorov, Orbital upper critical field and its anisotropy of clean one- and two-band superconductors, *Rep. Prog. Phys.* **75**, 114502 (2012).
- [37] R. Thomale, C. Platt, W. Hanke, J. Hu, and B. A. Bernevig, Exotic d -wave superconducting state of strongly hole-doped $K_xBa_{1-x}Fe_2As_2$, *Phys. Rev. Lett.* **107**, 117001 (2011).

Copyright of Physical Review B: Condensed Matter & Materials Physics is the property of American Physical Society and its content may not be copied or emailed to multiple sites or posted to a listserv without the copyright holder's express written permission. However, users may print, download, or email articles for individual use.